How to cite: *Angew. Chem. Int. Ed.* **2020**, *59*, 22132–22139
International Edition: doi.org/10.1002/anie.202008734
German Edition: doi.org/10.1002/ange.202008734

VIP **Structural Biology** *Very Important Paper*

Protein Allostery at Atomic Resolution

Dean Strotz, Julien Orts, Harindranath Kadavath, Michael Friedmann, Dhiman Ghosh, Simon Olsson, Celestine N. Chi, Aditya Pokharna, Peter Güntert, Beat Vögeli, and Roland Riek**

Abstract: *Protein allostery is a phenomenon involving the long range coupling between two distal sites in a protein. In order to elucidate allostery at atomic resoluion on the ligand-binding WW domain of the enzyme Pin1, multistate structures were calculated from exact nuclear Overhauser effect (eNOE). In its free form, the protein undergoes a microsecond exchange between two states, one of which is predisposed to interact with its parent catalytic domain. In presence of the positive allosteric ligand, the equilibrium between the two states is shifted towards domain–domain interaction, suggesting a population shift model. In contrast, the allostery-suppressing ligand decouples the side-chain arrangement at the inter-domain interface thereby reducing the inter-domain interaction. As such, this mechanism is an example of dynamic allostery. The presented distinct modes of action highlight the power of the interplay between dynamics and function in the biological activity of proteins.*

[*] Dr. D. Strotz, Dr. J. Orts, Dr. H. Kadavath, Dr. M. Friedmann, D. Ghosh, A. Pokharna, Prof. Dr. P. Güntert, Prof. Dr. R. Riek
Laboratory of Physical Chemistry,
Swiss Federal Institute of Technology, ETH-Hönggerberg
8093 Zürich (Switzerland)
E-mail: roland.riek@phys.chem.ethz.ch

Dr. S. Olsson
Department of Mathematics and Computer Science,
Freie Universität Berlin, Arnimallee 6, 14195 Berlin (Germany)

Dr. C. N. Chi
Department of Medical Biochemistry and Microbiology,
Uppsala Biomedical Center, Uppsala University
751 23 Uppsala (Sweden)

Prof. Dr. P. Güntert
Institute of Biophysical Chemistry,
Center for Biomolecular Magnetic Resonance, and
Frankfurt Institute for Advanced Studies,
J.W. Goethe-Universität
Max-von-Laue-Str. 9, 60438 Frankfurt am Main (Germany),
and
Graduate School of Science, Tokyo Metropolitan University
Hachioji, Tokyo 192-0397 (Japan)

Dr. B. Vögeli
Department of Biochemistry and Molecular Genetics,
University of Colorado at Denver
12801 East 17th Avenue, Aurora, CO 80045 (USA)
E-mail: beat.vogeli@cuanschutz.edu

Supporting information and the ORCID identification number(s) for the author(s) of this article can be found under: https://doi.org/10.1002/anie.202008734.

Introduction

Allostery in proteins describes the process by which a signal such as ligand binding on one site of a protein or protein complex is transmitted to another distal functional site thereby regulating biological activities.[1] Several models on the mechanism of allostery have been postulated including the sequential mechanism,[2] the population shift model (including the conformational selection mechanism originally termed the symmetric model; Monod[3]), and the dynamic allostery model.[4] While the sequential mechanism assumes adaptability of the structure upon ligand binding, the model by Monod is based on the existence of two pre-existing exchanging states whose population equilibrium shifts upon ligand binding since the ligand selects one of the two states. The dynamic allostery model assumes that ligand binding changes the frequency and amplitude of thermal fluctuations within a protein without perturbing the average structure.

Experimental elucidation of allostery as "an action at a distance" phenomenon is challenging.[1] The challenge is due to the availability of mostly low resolution, local data in NMR—including relaxation studies[5,6]—or individual determined structures of trapped states (such as free and ligand-bound states, or intermediate states stabilized by for example mutagenesis). Integrating analysis of experimental data with molecular dynamic simulations using for example recently developed statistical methods is however emerging as an interesting and powerful approach.[7–11]

Recent progress in NMR-based methods opened an avenue towards a more holistic description of motion and ensembles of structures. These include residual dipolar coupling (RDC) measurements, relaxation dispersion NMR experiments, cross-correlated relaxation (CCR), paramagnetic relaxation enhancement (PRE), and exact Nuclear Overhauser Enhancement or Effect (eNOE) data in combination with molecular dynamics simulation, structure prediction software, or ensemble-based structure calculations.[12–26]

Here, we made use of the eNOE approach, which allows for the multi-state structure determination of well behaving proteins because of the high accuracy (i.e. <0.1 Å) of the ensemble-averaged restraints obtained[23,25,27,28] and applied it to a variant of the prototypical allostery-comprising WW domain of Pin1 (see the Material and Methods section in the Supporting Information). Pin1 is a peptidyl-prolyl cis-trans isomerase (PPIase). Its biological significance includes amongst others an involvement in the regulation of mitosis,[29] a protective function against Alzheimer's disease,[30] increase of hepatitis C infection[31] and it is overexpressed in many human cancer cells.[32] Pin1 contains an N-terminal WW

domain (the name has its origin in the presence of two Trp residues) separated by a flexible linker from the C-terminal catalytic PPIase domain (Figure 1 A).[33]

The 34-residues-long N-terminal WW domain is thought to be responsible for ligand recognition and binding as evidenced by NMR titration experiments (Figure 1), the C-terminal domain contains the catalytically active site. The two domains, which interact loosely via Loop 2 of the WW domain (i.e. residues I28-Q33), form the ligand binding site and the extent of interaction depends on the ligand that binds at a distal Loop 1 comprising residues M15-R21.[34–36] One family of substrate (such as the peptide pCdc25C of interest here)

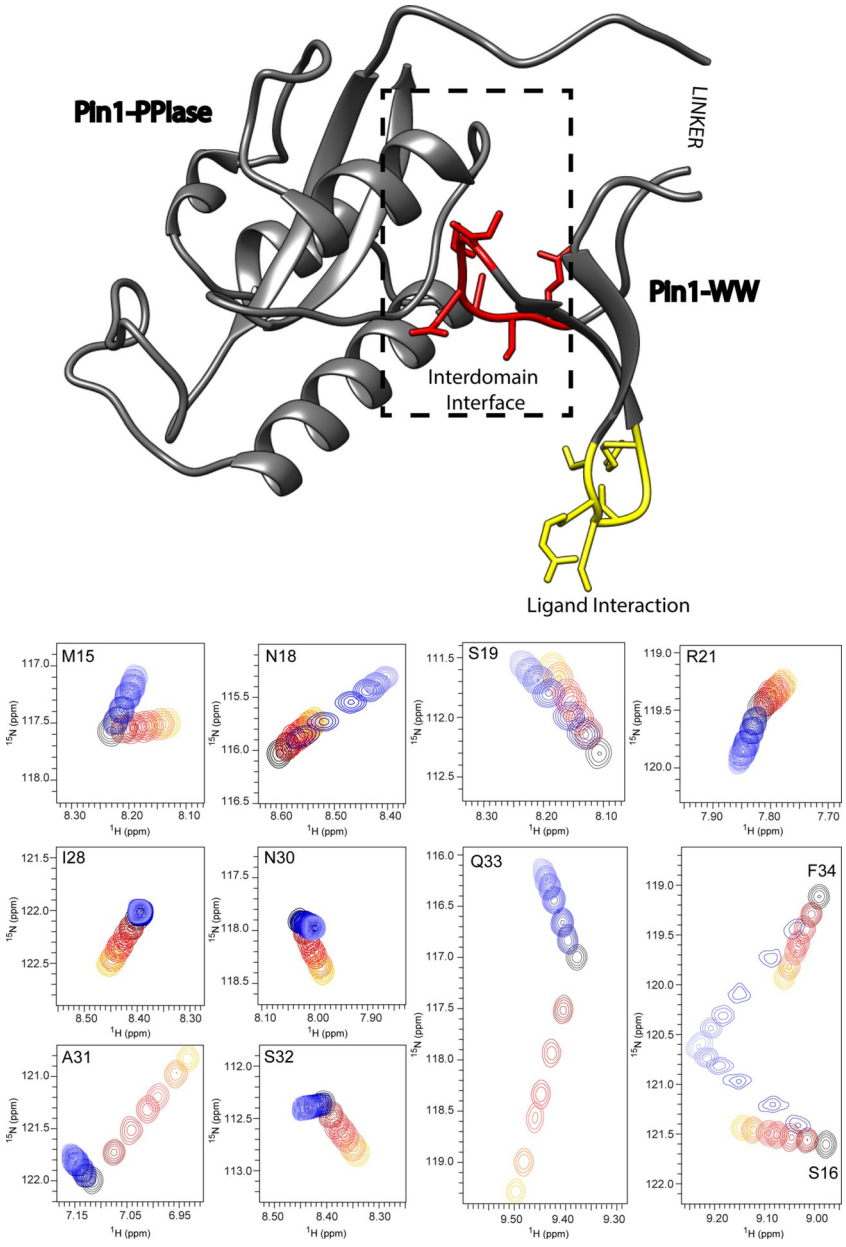

Figure 1. The 3D structure of Pin1 with its postulated allosteric interaction within the variant WW domain. The allostery within the WW domain occurs between the ligand-binding site (indicated in yellow) and the interaction site with its catalytic domain is highlighted in red and labeled as the inter-domain interface.[38–41,43–45] This interaction is shown on top of the 3D crystal structure (PDB code 1PIN) represented by a ribbon with the residues of interest also highlighted by side chains. The NMR chemical shift titrations of the ^{15}N-labeled variant WW with the positive allosteric peptide FFpSPR and the negative allosteric peptide pCdc25C are shown for the relevant residues (i.e. M15-R21 form the ligand binding site and I28-Q33 are residues in the inter-domain interface) measured by [^{15}N,^{1}H]-HSQC experiments. The black cross peak corresponds to the ^{15}N-^{1}H moiety of the apo form. Upon titration with FFpSPR highlighted by the color code ranging from black over red to yellow, the cross peaks move with increasing concentration away from the apo form. Similarly, the color changes from dark to light blue indicate the chemical shift changes due to the interaction with the ligand pCdc25C. The shift changes indicate a fast exchange regime (i.e. µs time regime). In the binding site, the cross peaks move in the same direction for both ligands, while at the interface they shift in opposite directions. While the interface peaks undergo smaller shifts for the negative-allosteric ligand pCdc25C in comparison with FFpSPR, the binding-site peaks show similar shift magnitudes.

reduces the inter-domain contact, while other peptide families (such as the peptide FFpSPR of interest here) enhance the inter-domain contact.[35,37,38] Extensive studies at low resolution by others show that these properties require a substantial allosteric cross-talk between Loop 2 and the ligand binding site Loop 1 of the WW domain.[38–45] Thus, the WW domain possesses a ligand-mediated allosteric coupling. Experimental evidence includes the ligand titration NMR experiments with the isolated WW domain, showing chemical shift changes at the distal site Loop 2 upon ligand binding at Loop 1 (Figure 1).[38–41,43–45] Furthermore, the two ligands induce distinct chemical shift changes in direction and magnitude on Loop 2 in line with their opposing property in the inter-domain interaction (Figure 1).[38] In order to explore the nature of this allosteric coupling at atomic resolution eNOE ensemble structures were determined of the apo-state of the WW domain as well as the WW domain in presence of either of the two peptide ligands FFpSPR and pCdc25C.

Results

Multi-State Structure Determination of the WW domain in Absence and Presence of Ligands

Following an established protocol[23,25] with the eNORA2 program[46] ([47] CYANA version), ensemble structure calculations were performed for all three systems with eNOE-based distance restraints (Figure 2A) and scalar couplings (Supplementary Tables S1–S3 and Material for more details). In Figure 2B, the large number of restraints is demonstrated for Trp11 in the apo form of the WW domain, for which ca. 60 distance restraints have been collected, while on average there are roughly 20 eNOE-derived distance restraints per residue. As a measure of the quality of the calculated structures, the CYANA target function (TF), which is a weighted sum of all squared violations of the experimental restraints, is used. It drops significantly from one state to two states and levels off after three states (Figure 2C). In a ten-state structure calculation, the two states are still observed (as exemplified in the Ramachandran plot for Thr29 in Figure S1) further supporting the two-state nature of the system. While the TF is an insensitive measure for determining the populations of the two states (Figure S2A), the details of

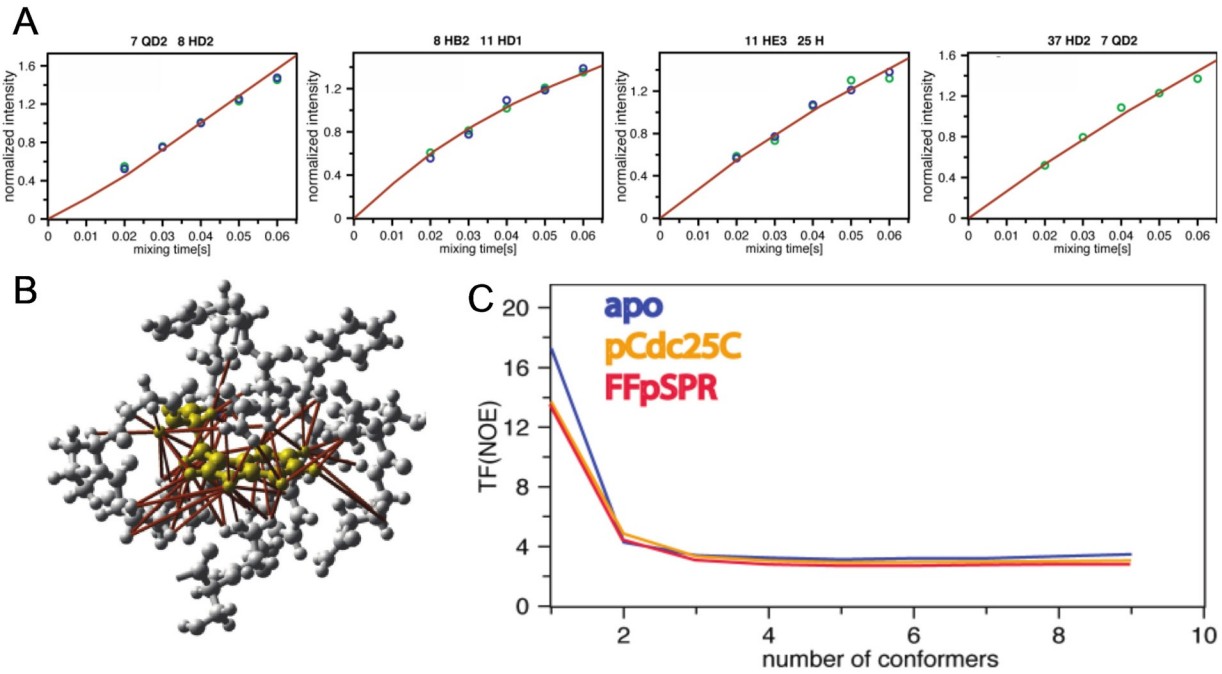

Figure 2. Distance restraint collection and structure calculation. A) Five experimental eNOE measured at 20, 30, 40, 50, and 60 ms NOESY mixing time of the apo WW domain, color coded by green and blue dots corresponding to the two respective NOEs on both sides of the diagonal versus time are shown. In addition, these data are superimposed with back-predicted buildups derived from the calculated two-state ensembles. The NOEs are between residues indicated at the top of each graph. The intensities are normalized to the average value of each buildup. The back-predicted theoretical model fulfils the experimental data very well (see also Figure S2). The back-predicted buildups were calculated using eNORA2 implemented in CYANA[46] ([47] CYANA version). B) eNOE-derived distance restraints around Trp11 of apo WW are mapped onto the 3D structure, indicating the large size of the data set. Trp11 and residues around Trp11 are shown in yellow and grey, respectively. Over 60 eNOE distance restraints (highlighted in red) were collected contrasting the four degrees of freedom of a Trp. This highlights the high density of information obtained by eNOE-based structure determination. C) CYANA target function (TF) values of various ensemble-based structure calculations, demonstrating the importance of the ensemble-based structure. The CYANA TF, which is the (weighted) sum of the squared violations of the conformational restraints versus number of simultaneously calculated states, is shown for all three calculations. The decrease of the TF with an increasing number of states indicates that at least two states are required to describe the experimental data well.

the two states are preserved (including the correlated/non-correlated configurations of Thr29 and Ala31 discussed below) for a population range 1:1—≈1:3 for apo WW and WW domain in complex with pCdc25C, while for WW—FFpSPR it is conserved in the range of 1:9–4:6 (Figure S2A).

In order to get further insights into the relative population of the two states, we conducted titration experiments with FFpSPR using a T2-filtered [^{15}N,^{1}H]-HSQC experiment to enhance the signal broadening. The broadest signal can be attributed to a 1:1 population allowing a determination of the relative populations of the two states of ≈1:3 for apo WW (Figure S2B). To support this finding a ^{15}N-resolved CEST—[^{15}N,^{1}H]-TROSY experiment was conducted for apo WW (Figure S2C). The CEST data of the allosteric sites Ala31 and Gln33 albeit at the noise level show the presence of two states, one corresponding to the fully FFpSPR-bound state (Figure S2C, blue arrow), while the other allosteric state can also be identified (Figure S2C, cyan arrow) and agrees well with the elucidation of the shifts of the two states by the titration (Figures S2B and S2C). With the knowledge of the chemical shifts of the samples used for the structure determination, it can be estimated that the two states of the apo WW domain are present in a ratio of ≈3:1, while in the WW-FFpSPR complex the populations are ≈1:4. ^{15}N relaxation measurements at two magnetic fields in concert with the titration experiments revealing the chemical shift difference between the two states yielded individual exchange rates (Figure S2D). A similar exchange rate of ca 100 kHz is observed for both the ligand binding site (i.e. Ser19) as well as the allosteric site (i.e. Ile28, Asn30, Ala31, Ser32, and Gln33) supporting again the presence of two states that exchange in a concerted fashion.

Overall, these findings indicate that, in contrast to the single-state structure, multi-state ensembles describe the experimental data well (Tables S1–S3).

Validating the Multi-State Structures

The agreement of the model with the experimental data is also illustrated by the superposition of experimental NOE data and back-calculated NOE buildups (Figure 2A). The improvement of the model with respect to the experimental data is shown even more explicitly by comparing back-predictions derived from single-state structures in comparison to the model derived from two-state structures (Figure S3). Furthermore, a cross-validation test with cross-correlated relaxation data (not used in the structure calculations) fit better with the two-state structural ensembles than the single-state structures (Figure S4). Finally, a cross-validation test was performed with a jackknife procedure that repeats the structure calculation twenty times with 5% of the experimental input data randomly deleted such that each distance restraint is omitted exactly once. These obtained structures are similar to the original structures including the correlated states between Thr29 and Ala31 of interest below (Figure S5). As a representative for the following discussion, the two state ensembles described by a structural bundle of 2×20 conformers (Figure 2) are used.

Discussion

The Apo State of the WW Domain Comprises Two Distinct Conformational States

Inspection of the apo WW domain two-states ensemble reveals two spatially well-separated states from the ligand-binding site including Loop 1 via the backbone of the β-strand β2 and Asn26 to the inter-domain site Loop 2 (Figure 3A). The two states are well separated both by the side chains shown (i.e. Arg14, Met15, Ser16, Ser19, Tyr23, Phe25, Asn26, Ile28, Thr29, Asn30, Ala31, Gln33) as well as the backbone angles for Thr29 and Ala31 highlighted in Ramachandran plots (Figure S6). Since only one set of chemical shifts is observed, it is suggested that the two states interchange in the micro-millisecond time range in a concerted fashion between the side chain of the ligand binding site (such as Arg14, Met15, Ser16, Ser19, Tyr23 and possibly Phe25) to the side chains of the inter-domain interaction site (i.e. Ile28, Thr29, Asn30, Ala31 and Gln33) via the backbone of the β-strand β2 and the side chain Asn26 (Figure 3A). Of particular interest for the following comparison is thereby the relative side-chain arrangements of Thr29 and Ala31 side chains (Figures 3A and D), which can be illustrated by a seesaw sketch representing the two states (Figures 3D and F): if the side chain of Thr29 is "below" the backbone in Figure 3D, the side chain of Ala31 is "above" it and vice versa if the side chain of Thr29 is "above" the backbone, the side chain of Ala31 is "below" it, respectively.

The Mechanism of Action of the Positive Allosteric Ligand Shifts the Population of States

Inspection of the two-state structure of the WW domain in complex with the positive allosteric ligand FFpSPR shows that the two-state ensemble of the WW domain only shifts the population of the two states towards the dark blue state identified in the apo form (Figures 3A and D). This includes the seesaw arrangement (Figure 3E) between the two side chains of Thr29 and Ala31 as illustrated in Figure 3D for which the yellow state of the complex superimposes well with the cyan state of the apo WW, while the red state of the complex superimposes well with the blue state of the apo WW domain. These arrangements are also found in the Ramachandran plots of Thr29 and Ala31 (Figure S6). Thus, the FFpSPR peptide appears to select the dark blue state such that the mode of allosteric action is proposed to be conformational selection.[3]

The Negative Allosteric Ligand Follows the Dynamic Allostery Model

In striking contrast to the peptide FFpSPR, peptide pCdc25C influences the inter-domain interaction between the WW domain and its catalytic domain negatively. Based on the finding that the peptide FFpSPR acts by the conformational selection model discussed above, it would seem logical to

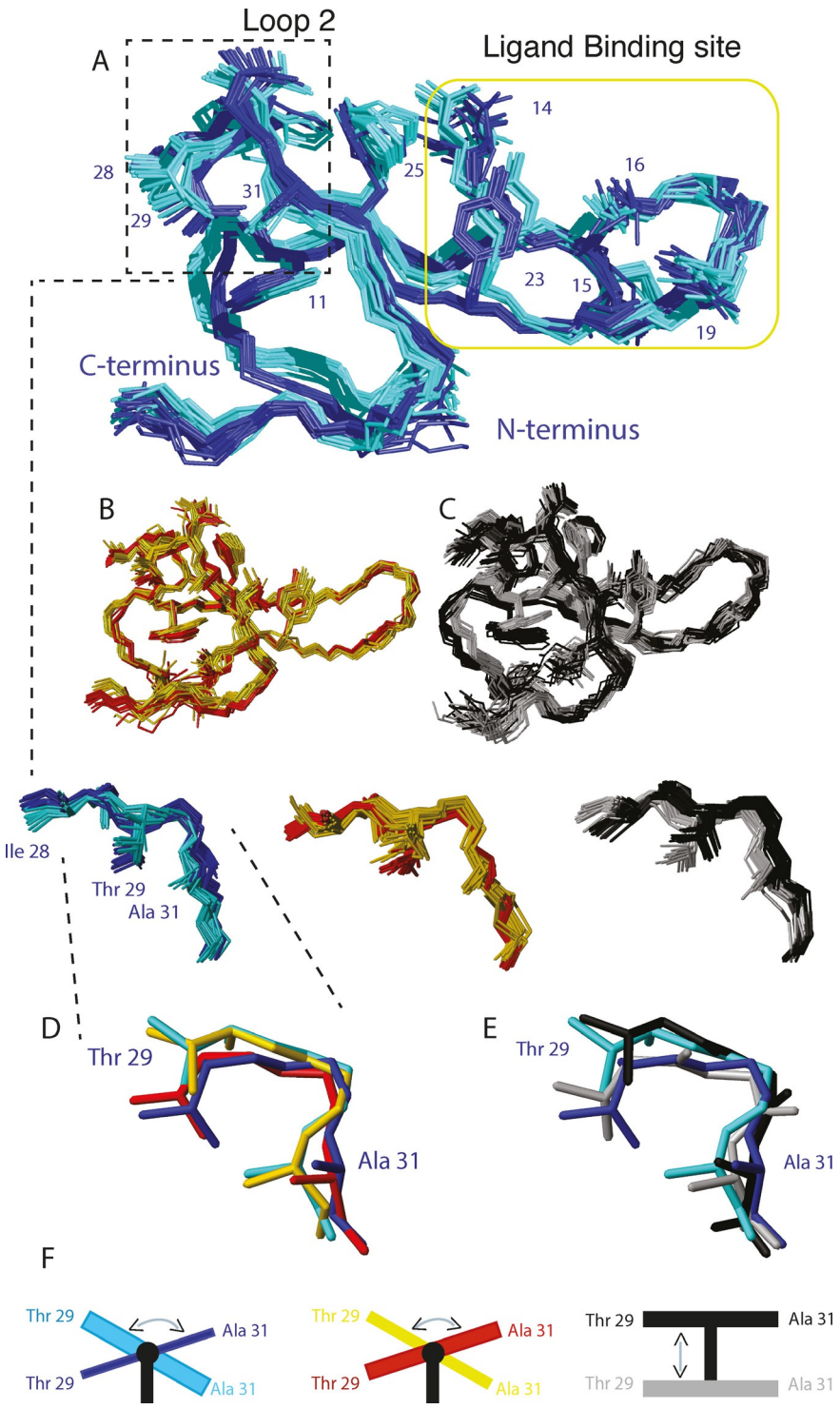

Figure 3. Two-state structural ensemble of apo WW (A), WW in complex with the positive (B) and negative (C) allosteric ligand, highlighting the presence of two distinct states. Backbone traces of 20 structural ensembles of the WW domain each representing two different states are shown. In addition, several side chains are shown and labeled. The WW states are color coded with cyan and blue for the apo WW, yellow and red for the positive allosteric ligand FFpSPR complex, and grey and black for the negative allosteric ligand pCdc25C complex. The two states of the catalytic-domain-interacting Loop 2 are enlarged as indicated. In addition, the two states for residues 29–31 are shown for one conformer only for clarity in (D) and (E) by superimposing the two apo states with either the two states of the positive (D) or the two states of the negative (E) allosteric-ligand–WW complex. These superpositions illustrate that the positive allosteric ligand does not alter the two-state structures as the yellow state superimposes with the cyan state and the red state with the blue state for both residues Thr29 and Ala31. In the case of the negative allosteric ligand, the grey state superimposes with the blue state for residue Thr29, but for Ala31, the blue state superimposes with the black state, and the black state superimposes with the cyan state for Thr29, while the black state superimposes with blue state of Ala31. In (F) this observed change is illustrated by a seesaw model. In the case of apo WW, Thr29 and Ala31 alter their states like a seesaw with the cyan state more populated (drawn thicker). When bound to the positive allosteric ligand, the seesaw states are preserved, however with different populations of the two states. In contrast, no seesaw-like two states are observed in the case of the negative allosteric ligand, shown in grey/black.

assume that the pCdc25C peptide selects the binding-incompetent state and thereby interferes with the inter-domain interaction. However, this is not the case as revealed by the two-state structure calculation of the WW domain in presence of the peptide ligand pCdc25C. Still, two states are observed (Figure 2C). Furthermore, both states are distinct in the backbone (represented by Ramachandran plots in Figure S6) as well as the side chains of Loop 2 (Figure 3C and D). However, the backbone and side-chain states in Loop 2 between residues Ile28/Thr29 versus Ala31 are anti-correlated with each other when compared with the apo structure and the FFpSPR structure (Figure 3D). Hence, the two states of the seesaw of the Thr29/Ala31 side chains do not exist anymore but either both side chains are up or down simultaneously as illustrated in Figure 3D and E. In detail, when the side chain of Thr29 is close to the dark blue state of the apo structure, the side chain of Ala31 is superimposable with the cyan state, while if the side chain of Ala31 is close to the cyan apo structure, the side chain of Thr29 aligns with the dark blue state of the apo structure. Thus, when Loop 2 is locally averaged over the two states the apo structure is locally not distinguishable from the WW domain structure in complex with pCdc25C as supported by minor observed chemical shift changes contrasting the situation for the positive allosteric case (Figure 1). However, when viewed in a time-resolved manner the free WW domain and in complex behave differently because the dynamics altered. The pCdc25C peptide—WW domain complex can thus be regarded as an example of a dynamic allostery model, where the local structure is not perturbed on average, but on the global level there is a change from a correlated motion in the apo-state to an anticorrelated motion in the complex (Figure 3D and E).

The Ligand-Induced Allostery of the WW Domain in the Context of Full-Length Pin1

It has been demonstrated that by binding to Loop 1 of the WW domain the peptide pCdc25C reduces the loose inter-domain contact with the C-terminal catalytic PPIase domain via an allosteric mechanism,[33] while the peptide FFpSPR enhances this inter-domain contact.[35,37,38] Since Loop 2 is the side of the WW domain which interacts with the PPIase domain, the above findings on the two states on Loop 2 (Figure 3) give insights into the mechanism of positive and negative influence on the interaction between the two domains. For this the WW domain structures of all three systems studied here were superimposed with the WW domain of the crystal structure of full-length Pin 1 (Figure 4; 1PIN.pdb). The superpositions show that the cyan and yellow states of the apo WW and WW domain in complex with FFpSPR clash in part with the catalytic PPIase domain in contrast to the corresponding blue and red states, respectively. Since the predicted clash is not possible because of very large van der Waals energies, it is assumed that the cyan and yellow states are not fit in binding with the catalytic PPIase domain. Indeed, upon FFpSPR peptide ligand binding the population changes in favor of the red non-clashing state and thus the inter-domain interaction is enhanced as demonstrated.[35,37,38] In the case of the WW domain bound with pCdc25C both states clash into the catalytic domain, which is interpreted that both states are not able to interact well with the catalytic domain as demonstrated.[35,37,38]

The mechanism of the allosteric coupling between ligand-binding Loop 1 and inter-domain interacting Loop 2 is further illustrated in Figure 5 (clay colored structure). The WW domain possesses two distinct states likely of similar energy that cover both the ligand binding site (i.e. Loop 1) as well as the inter-domain interacting site (i.e. Loop 2). The inter-change between the catalytic domain-binding competent and non-competent states of Loop 2 in the micro-second time

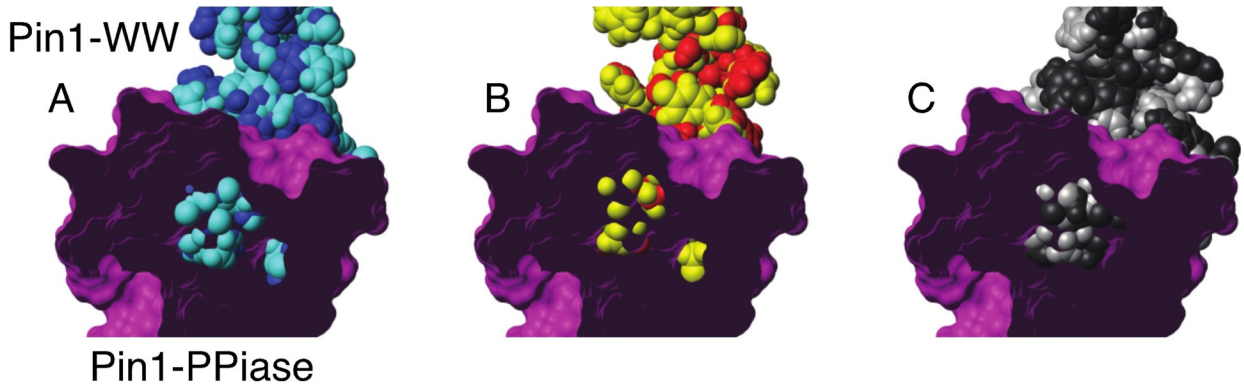

Figure 4. The multi-state structures of the WW domain in the context of its predicted interaction with the catalytic domain highlight state-specific clashes. The two-state structures are shown by space filling calotte (CPK) models of A) the apo WW in cyan and blue, B) the WW domain in complex with the positive allosteric ligand FFpSPR (shown in yellow and red), and C) the WW domain in complex with the negative allosteric peptide pCdc25C (shown in grey and black), which have been superimposed onto the WW domain structure of full-length Pin1 (PDB code 1PIN). The contact surface of the catalytic domain Pin1-PPIase is shown in pink, cut from the front in order to illustrate the eventual clashing of the WW domain with the Pin1-PPIase domain. Note, there is only a clash if the center of the spheres of the WW domain are visible inside the PPIase. The inspection of the figures shows that in (A) the cyan state clashes with the pink PPIase domain, while the blue state does not; in (B) the yellow state clashes with the PPIase domain, while the red state does not, and in (C) both the black and grey states clash with the PPIase domain.

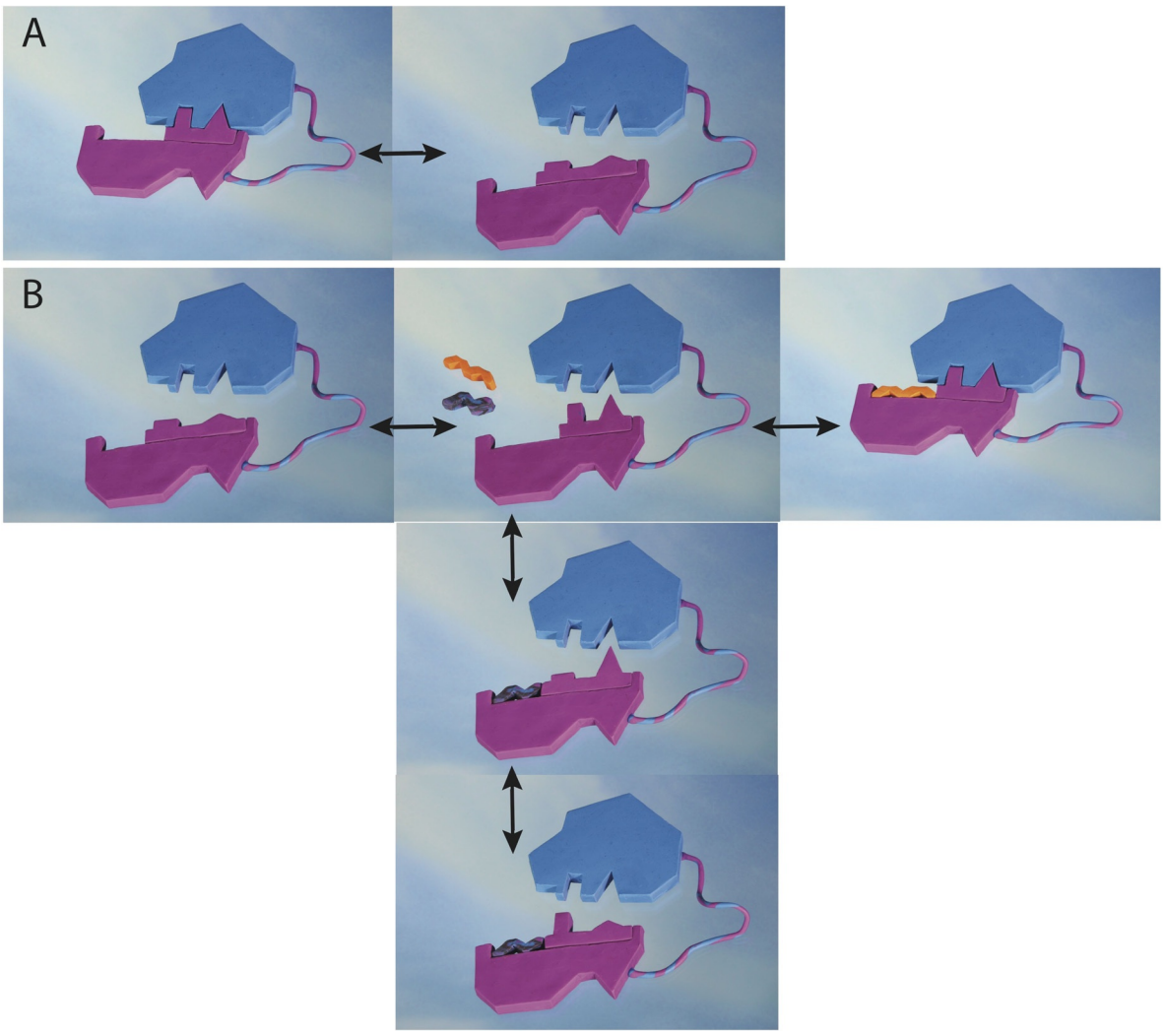

Figure 5. Allosteric mechanisms of action of the WW domain. A) The apo form of the WW domain (represented by a pink clay form) is undergoing exchange between two states, one of which (on the left) is able to bind the catalytic domain colored in blue. B) In presence of either the positive allosteric ligand FFpSPR (shown in orange) or the negative allosteric peptide pCdc25C (shown in black) two distinct allosteric mechanisms are active. The positive allosteric ligand FFpSPR selects the state that interacts with the catalytic domain, enhancing interaction with the catalytic domain (arrow to the right). This proposed mechanism is thus based on the population shift model. The negative allosteric peptide pCdc25C acts via the dynamic allostery model, where the average local structure is not perturbed, but at any given time it is incompatible with interacting with the catalytic site.

range of the apo WW domain thereby perturbs the inter-domain contact. The ligand FFpSPR selects the binding-competent state and enhances the inter-domain interaction. In contrast, in complex with pCdc25C both Loop 2 conformations show clashes interpreted here as interference of a domain–domain interaction (Figure 5). While the average structure of Loop 2 did not get perturbed upon pCdc25C binding (in Figure 5: the two triangles and two rectangles are on average the same as in the apo state) it is the dynamics that changed from being concerted in the apo state to anti-correlated in the complex with pCdc25C yielding binding interference to the catalytic domain. Hence, depending on the peptide not only the outcome of allostery but also the mechanism of allostery is altered. This is possible since all the structural states involved have similar energies with low activation barriers between them enabling different processes and pathways by small perturbations.

Conclusion

There are several mechanisms of action of allostery including the population shift model and the dynamic allostery model. Because of recent advances in NMR methodology a large collection of highly accurate experimental data was obtained and allowed to elucidate the mechanism of allostery for the WW domain at atomic resolution. A ligand-dependent mechanism of action of allostery was thereby revealed, inferring for one ligand the population shift model and for the other ligand the dynamic allostery model. These mechanisms of action highlight also the possible multi-dimensional interplay between dynamics and structure that amount to evolutionary selection for fittest performance. It further indicates the astonishing multifaceted possibilities this multi-dimensional dynamic structure landscape possesses.

Conflict of interest

The authors declare no conflict of interest.

Keywords: allostery · ligand binding · NMR spectroscopy · protein dynamics · protein structure

[1] H. N. Motlagh, J. O. Wrabl, J. Li, V. J. Hilser, *Nature* **2014**, *508*, 331 – 339.
[2] D. E. Koshland, G. Nemethy, D. Filmer, *Biochemistry* **1966**, *5*, 365 – 385.
[3] J. Monod, J. P. Changeux, F. Jacob, *J. Mol. Biol.* **1963**, *6*, 306 – 329.
[4] A. Cooper, D. T. F. Dryden, *Eur. Biophys. J. Biophys. Lett.* **1984**, *11*, 103 – 109.
[5] L. E. Kay, *J. Magn. Reson.* **2005**, *173*, 193 – 207.
[6] L. E. Kay, D. A. Torchia, A. Bax, *Biochemistry* **1989**, *28*, 8972 – 8979.
[7] W. C. Swope, J. W. Pitera, F. Suits, M. Pitman, M. Eleftheriou, B. G. Fitch, R. S. Germain, A. Rayshubski, T. J. C. Ward, Y. Zhestkov, R. Zhou, *J. Phys. Chem. B* **2004**, *108*, 6582 – 6594.
[8] F. Noé, D. Krachtus, J. C. Smith, S. Fischer, *J. Chem. Theory Comput.* **2006**, *2*, 840 – 857.
[9] D. E. Shaw, P. Maragakis, K. Lindorff-Larsen, S. Piana, R. O. Dror, M. P. Eastwood, J. A. Bank, J. M. Jumper, J. K. Salmon, Y. B. Shan, W. Wriggers, *Science* **2010**, *330*, 341 – 346.
[10] S. Olsson, F. Noe, *J. Am. Chem. Soc.* **2017**, *139*, 200 – 210.
[11] S. Olsson, H. Wu, F. Paul, C. Clementi, F. Noe, *Proc. Natl. Acad. Sci. USA* **2017**, *114*, 8265 – 8270.
[12] J. R. Tolman, J. M. Flanagan, M. A. Kennedy, J. H. Prestegard, *Nat. Struct. Biol.* **1997**, *4*, 292 – 297.
[13] L. Yao, B. Vögeli, D. A. Torchia, A. Bax, *J. Phys. Chem. B* **2008**, *112*, 6045 – 6056.
[14] P. Vallurupalli, D. F. Hansen, L. E. Kay, *Proc. Natl. Acad. Sci. USA* **2008**, *105*, 11766 – 11771.
[15] P. Neudecker, A. Zarrine-Afsar, A. R. Davidson, L. E. Kay, *Proc. Natl. Acad. Sci. USA* **2007**, *104*, 15717 – 15722.
[16] E. J. Fuentes, S. A. Gilmore, R. V. Mauldin, A. L. Lee, *J. Mol. Biol.* **2008**, *375*, 1489 – 1490.
[17] E. J. Fuentes, C. J. Der, A. L. Lee, *J. Mol. Biol.* **2004**, *335*, 1105 – 1115.
[18] A. Dhulesia, J. Gsponer, M. Vendruscolo, *J. Am. Chem. Soc.* **2008**, *130*, 8931 – 8939.
[19] G. M. Clore, C. D. Schwieters, *J. Am. Chem. Soc.* **2004**, *126*, 2923 – 2938.
[20] G. M. Clore, C. D. Schwieters, *Biochemistry* **2004**, *43*, 10678 – 10691.
[21] K. Lindorff-Larsen, R. B. Best, M. A. DePristo, C. M. Dobson, M. Vendruscolo, *Nature* **2005**, *433*, 128 – 132.
[22] G. Bouvignies, P. Bernado, S. Meier, K. Cho, S. Grzesiek, R. Bruschweiler, M. Blackledge, *Proc. Natl. Acad. Sci. USA* **2005**, *102*, 13885 – 13890.
[23] B. Vögeli, S. Kazemi, P. Güntert, R. Riek, *Nat. Struct. Mol. Biol.* **2012**, *19*, 1053 – 1057.
[24] N. A. Lakomek, K. F. A. Walter, C. Fares, O. F. Lange, B. L. de Groot, H. Grubmuller, R. Bruschweiler, A. Munk, S. Becker, J. Meiler, C. Griesinger, *J. Biomol. NMR* **2008**, *41*, 139 – 155.
[25] C. N. Chi, D. Strotz, R. Riek, B. Vögeli, *J. Biomol. NMR* **2015**, *62*, 63 – 69.
[26] S. Olsson, D. Strotz, B. Vogeli, R. Riek, A. Cavalli, *Structure* **2016**, *24*, 1464 – 1475.
[27] P. J. Nichols, A. Born, M. A. Henen, D. Strotz, J. Orts, S. Olsson, P. Güntert, C. N. Chi, B. Vögeli, *Molecules* **2017**, *22*, 1176.
[28] P. J. Nichols, A. Born, M. A. Henen, D. Strotz, C. N. Celestine, P. Güntert, B. Vögeli, *ChemBioChem* **2018**, *19*, 1695 – 1701.
[29] K. P. Lu, S. D. Hanes, T. Hunter, *Nature* **1996**, *380*, 544 – 547.
[30] S. L. Ma, L. Pastorino, X. Z. Zhou, K. P. Lu, *J. Biol. Chem.* **2012**, *287*, 6969 – 6973.
[31] Y. S. Lim, H. T. L. Tran, S. J. Park, S. A. Yim, S. B. Hwang, *J. Virol.* **2011**, *85*, 8777 – 8788.
[32] K. Lu, *Cancer Cell* **2003**, *4*, 175 – 180.
[33] R. Ranganathan, K. P. Lu, T. Hunter, J. P. Noel, *Cell* **1997**, *89*, 875 – 886.
[34] E. Bayer, S. Goettsch, J. W. Mueller, B. Griewel, E. Guiberman, L. M. Mayr, P. Bayer, *J. Biol. Chem.* **2003**, *278*, 26183 – 26193.
[35] K. A. Wilson, J. J. Bouchard, J. W. Peng, *Biochemistry* **2013**, *52*, 6968 – 6981.
[36] J. J. Guo, X. D. Pang, H. X. Zhou, *Structure* **2015**, *23*, 237 – 247.
[37] D. M. Jacobs, K. Saxena, M. Vogtherr, P. Bernado, M. Pons, K. M. Fiebig, *J. Biol. Chem.* **2003**, *278*, 26174 – 26182.
[38] J. W. Peng, *Biophys. Rev.* **2015**, *7*, 239 – 249.
[39] T. Peng, J. S. Zintsmaster, A. T. Namanja, J. W. Peng, *Nat. Struct. Mol. Biol.* **2007**, *14*, 325 – 331.
[40] J. W. Peng, B. D. Wilson, A. T. Namanja, *J. Biomol. NMR* **2009**, *45*, 171 – 183.
[41] F. Morcos, S. Chatterjee, C. L. McClendon, P. R. Brenner, R. López-Rendón, J. Zintsmaster, M. Ercsey-Ravasz, C. R. Sweet, M. P. Jacobson, J. W. Peng, J. A. Izaguirre, *PLoS Comput. Biol.* **2010**, *6*, e1001015.
[42] R. B. Fenwick, L. Orellana, S. Esteban-Martin, M. Orozco, X. Salvatella, *Nat. Commun.* **2014**, *5*, 4070.
[43] J. C. Crane, E. K. Koepf, J. W. Kelly, M. Gruebele, *J. Mol. Biol.* **2000**, *298*, 283 – 292.
[44] M. Socolich, S. W. Lockless, W. P. Russ, H. Lee, K. H. Gardner, R. Ranganathan, *Nature* **2005**, *437*, 512 – 518.
[45] W. P. Russ, D. M. Lowery, P. Mishra, M. B. Yaffe, R. Ranganathan, *Nature* **2005**, *437*, 579 – 583.
[46] J. Orts, B. Vögeli, R. Riek, *J. Chem. Theory Comput.* **2012**, *8*, 3483 – 3492.
[47] D. Strotz, J. Orts, C. N. Chi, R. Riek, B. Vögeli, *J. Chem. Theory Comput.* **2017**, *13*, 4336 – 4346.

Manuscript received: June 22, 2020
Revised manuscript received: July 23, 2020
Accepted manuscript online: August 14, 2020
Version of record online: September 30, 2020

